nature physics

SUPPLEMENTARY INFORMATION

DOI: 10.1038/NPHYS3145

Wettability-independent bouncing on flat surfaces mediated by thin air films

Jolet de Ruiter, Rudy Lagraauw, Dirk van den Ende, Frieder Mugele

1. Drop bouncing series for various fluids: side and bottom views

Drop bouncing series are observed for various fluids and substrates. The latter include hydrophilic glass wafers, glass wafers hydrophobized with a UV-cured silicone oil layer, and glass wafers (super)hydrophobized by applying a nano-roughness in SU8 which is subsequently coated with a C_4F_8 layer, see also the Methods section. To show the universality of the bouncing phenomenon for both polar and non-polar liquids of a wide range of surface tensions, we tested seven different fluids as listed in Table S1. The surface tension ranges from 64.6 mN/m for water with a small amount (0.01 wt%) of rhodamin B to suppress reflections, down to 16 mN/m for fluorinert FC-40. The drops are formed at a precision needle with an outer diameter of 0.24 mm. They are detached by their own weight, yielding millimetre-sized radii depending on the density and surface tension of each fluid: radii vary between 0.52 mm for the low surface tension FC-40, and 1.03 mm for water. Although we are mainly interested in the influence of inertia and surface tension, we also keep track of the Bond number $Bo = \rho g R_0^2/\sigma$ and the Ohnesorge number $Oh = \mu(\sigma\rho R_0)^{-1/2}$ that give the ratio of gravity and viscosity to surface tension. The influence of viscosity is generally small, except for 85% wt. glycerol and sunflower oil, while gravity determines the equilibrium shape during the hovering phase.

Liquid	σ (mN/m)	ρ (kg/m^3)	μ (mPas)	R_0 (mm)	Bo (-)	Oh (-)
water	64.6	996.9	1.0	1.03	0.16	0.004
85% wt. glycerol	63.9	1219.4	~109	0.95	0.17	0.401
sunflower oil	33	920	~49	0.84	0.19	0.307
90% wt. propanol	28.7	825.2	2.2	0.79	0.17	0.016
decane	24	730	0.92	0.78	0.18	0.008
silicone oil	19.7	913	5	0.69	0.22	0.045
FC-40	16	1855	2.2	0.52	0.30	0.018

Table S1| Tested liquids. The liquid properties: surface tension σ, density ρ, and viscosity μ, are measured or obtained from specifications, while the drop radius R_0 is obtained from the side view recordings. The non-dimensional numbers give the ratio of gravity (Bond number $Bo = \rho g R_0^2/\sigma$) and viscosity ($Oh = \mu(\sigma\rho R_0)^{-1/2}$) to surface tension.

DOI: 10.1038/NPHYS3145

Movies S1 to S8 show bouncing series of droplets with various fluid properties and either a wettable or hydrophobic surface. Please note that these movies are a representative selection *not* necessarily recorded at the maximum possible initial Weber number. Table S2 summarizes the different experiments shown in the movies, together with the velocity v and Weber number of the initial impact We_{init}, the final Weber number obtained in the movie We_{end}, and the total timespan of the bouncing series. The substrate is a plasma treated glass wafer unless otherwise specified. The equilibrium contact angle on the substrate is also specified for all liquids in Table S2.

	Experiment	v (m/s)	We_{init} (-)	We_{end} (-)	time span (s)	θ_Y (°)
Movie S1	water	0.22	0.76	0.004	0.85	3
Movie S2	water/ wafer coated with cured silicone oil	0.20	0.64	0.023	0.50	90
Movie S3	85% wt. glycerol	0.21	0.83	0.003	0.16	9
Movie S4	sunflower oil	0.39	3.6	0.001	0.22	29
Movie S5	90% wt. propanol	0.37	3.0	0.011	0.40	~ 0
Movie S6	decane	0.36	3.1	0.003	0.69	~ 0
Movie S7	silicone oil	0.26	2.2	0.003	0.62	~ 0
Movie S8	FC-40	0.27	4.3	< 0.001	0.68	~ 0

Table S2| Summary of side-view movies showing bouncing series for various liquid/ substrate combinations. For each experiment the initial velocity v and the Weber number of the initial impact W_{init} are shown, as well as the final Weber number obtained in the movie W_{end} and the total timespan of the movie (all 40× delayed). The equilibrium contact angle θ_Y is measured in an independent experiment with a gently deposited drop.

All fluids show a very similar bouncing behaviour, in which the apparent contact angle remains virtually 180° during each bouncing event. A direct visualization of the air film using reflection interference microscopy confirms that no contact is made at all. A selection of bottom view movies – corresponding to a selection of the side view movies listed in Table S1 – is shown in Movies S9 to S11 for drops of water, sunflower oil, and 90% wt. propanol. In each movie, panel a shows the first bounce obtained at We_{init} as mentioned in Table S1, while panel b shows the full hover phase with progressively decreasing Weber number.

(a) 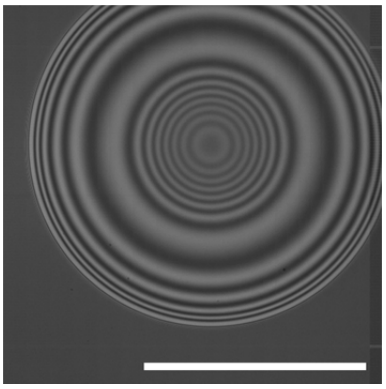 (b) 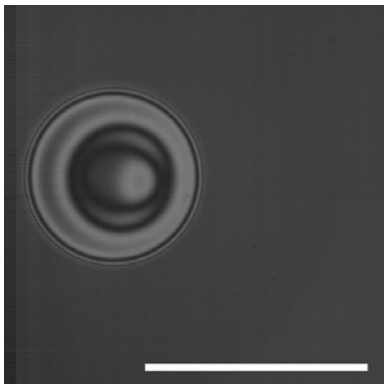

Movie S9| Persisting interference pattern proving the absence of contact: impact of a water droplet. See Movie S1 for the side view. (a) First bounce at $W_{init} = 0.76$, and (b) hover phase with We decreasing from 0.02 to 0.005. The total timespan is (a) 9.3 ms, and (b) 226 ms (both 667× delayed). The scale bar is 1 mm.

(a) 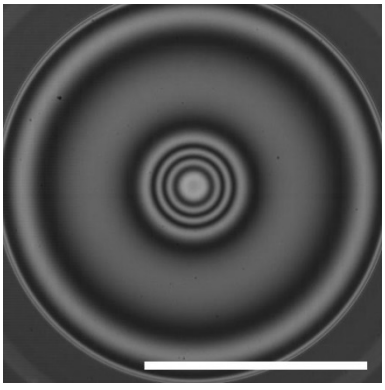 (b) 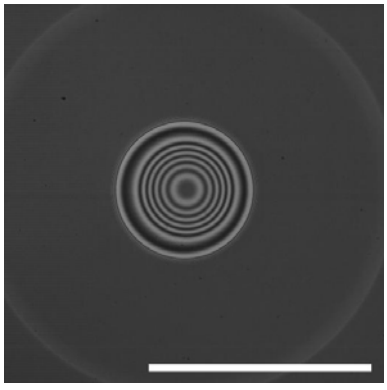

Movie S10| Persisting interference pattern proving the absence of contact: impact of a sunflower oil droplet. See Movie S4 for the side view. (a) First bounce at $W_{init} = 3.6$, and (b) hover phase with We decreasing from 0.049 to 0.001. The total timespan is (a) 8.9 ms, and (b) 102 ms (both 667× delayed). The scale bar is 1 mm. Reflections are visible as no rhodamin was added to the sunflower oil.

(a) 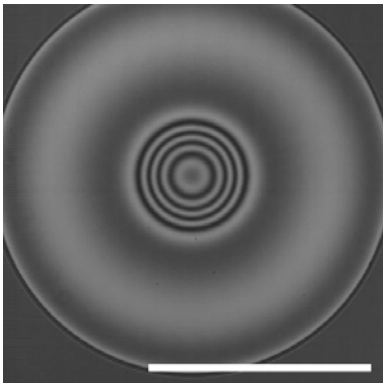 (b) 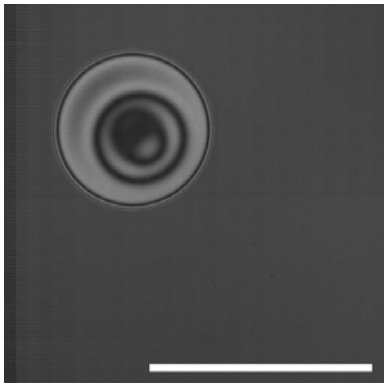

Movie S11| Persisting interference pattern proving the absence of contact: impact of a 90% wt. propanol droplet. See Movie S5 for the side view. (a) First bounce at $W_{init} = 3.0$, and (b) hover phase with We decreasing from 0.033 to 0.011. The total timespan is (a) 9.2 ms, and (b) 76 ms (both 667× delayed). The scale bar is 1 mm.

DOI: 10.1038/NPHYS3145

2. Centre of mass trajectories and decrease of Weber number

From each side view movie we extract a centre of mass (CM) trajectory, see Figure S1. The hovering phase roughly starts when the CM drops permanently below R_0. The water drop (Movie S1) exhibits the largest number of bounces and is analysed in more detail in the Letter. No trend with surface tension is observed; rather we obtain few bounces for the high-viscosity fluids where a significant amount of dissipation is associated with the internal flow field within the liquid.

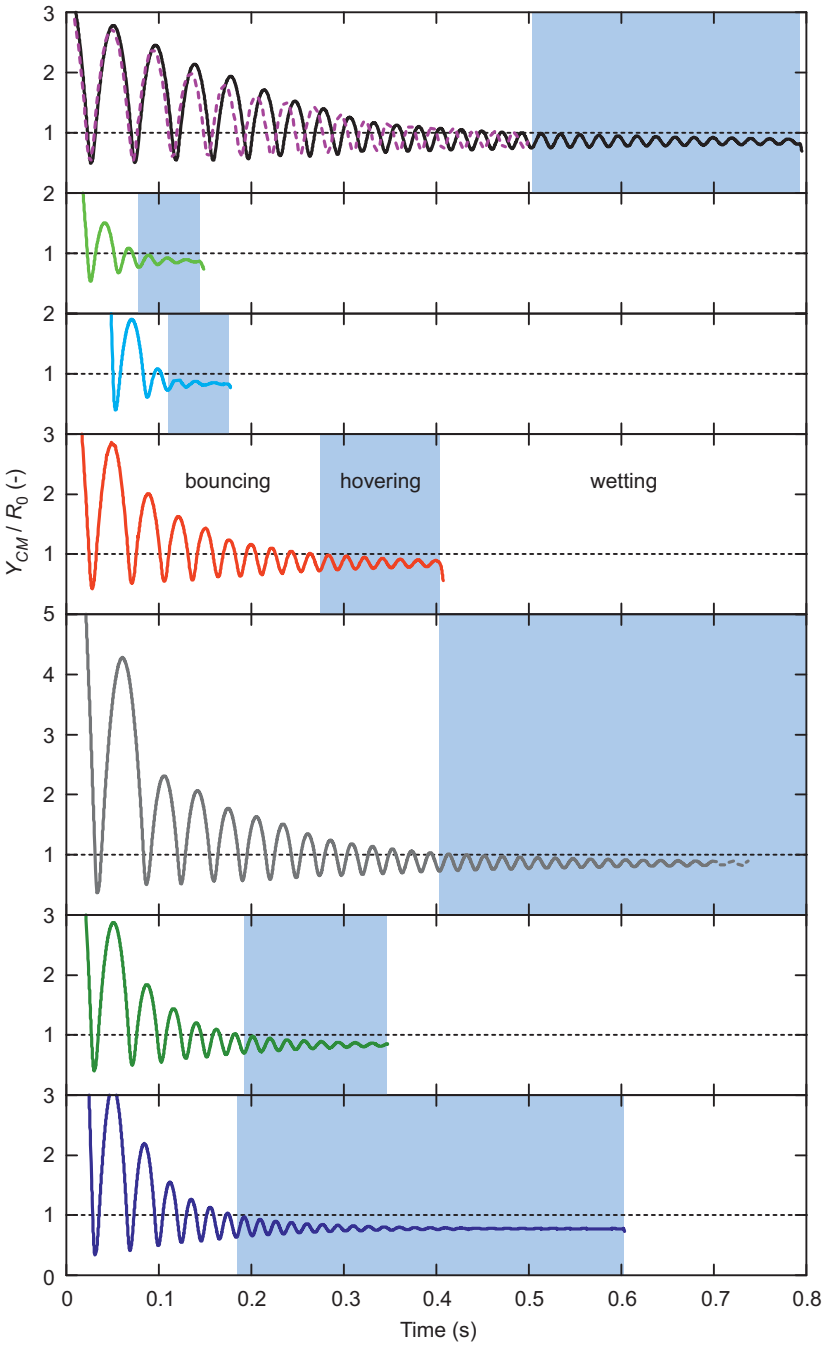

Figure S1| Centre of mass trajectories. From top to bottom, see Table S2: (black, magenta dashed) water on hydrophilic and hydrophobic wafer, respectively; (green) 85% wt. glycerol, (cyan) sunflower oil, (red) 90% wt. propanol, (grey) decane, (olive) silicone oil, (dark blue) FC-40. Blue shaded areas indicate the hovering phase.

Figure S2 illustrates the inherent decrease of We during a bouncing series for experiments with various liquids. The Weber number of each subsequent bouncing event is defined based on the maximum velocity reached just before the impact. Here, we selected for each fluid a recording with the highest initial impact velocity that still yielded a bouncing series. The data in Figure S2 can be re-plotted in a map of bouncing and hovering events versus surface tension and We number: Figure 3 in the Letter. There, if applicable we extracted the longest observed hovering phase from a separate experiment of the same fluid, to show the maximum width of the no-contact regime. The pixel resolution of the side-view sets a detection limit for hover oscillations that are too small to resolve ($We \approx 0.0001$). We can conclude that hovering persists down to at least $We \approx 0.001$.

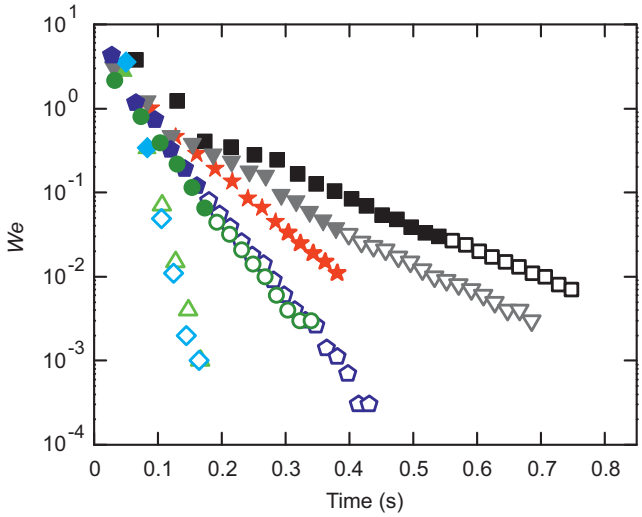

Figure S2| Decrease of Weber number during a bouncing series of various liquids. Solid symbols indicate the bouncing phase, open symbols the hover phase for experiments on smooth glass substrates with drops of: (black squares) water; (green triangles up) 85% wt. glycerol; (cyan diamonds) sunflower oil; (red stars) 90% wt. propanol; (grey triangles down) decane; (olive circles) silicon oil; and (dark blue pentagons) FC-40.

3. Restitution coefficient

The restitution of the bounce given by $\varepsilon = v'/v$, with v and v' the maximum absolute value of the velocity before and after the impact, is shown in Figure S3. It has a remarkably high average value of order 0.95 for $We \ll 1$. The restitution slightly increases during the bouncing and hovering phases and shows clear oscillation with We number that are likely attributed to the phase of the in-flight droplet oscillations with respect to impact [1]. For $We \geq 1$ the restitution coefficient sharply drops; in particular Biance *et al*. [1] have shown that the velocity after the bounce is independent of the initial impact velocity, leading to an immediate jump to $We \approx 1$ for the second bounce.

DOI: 10.1038/NPHYS3145

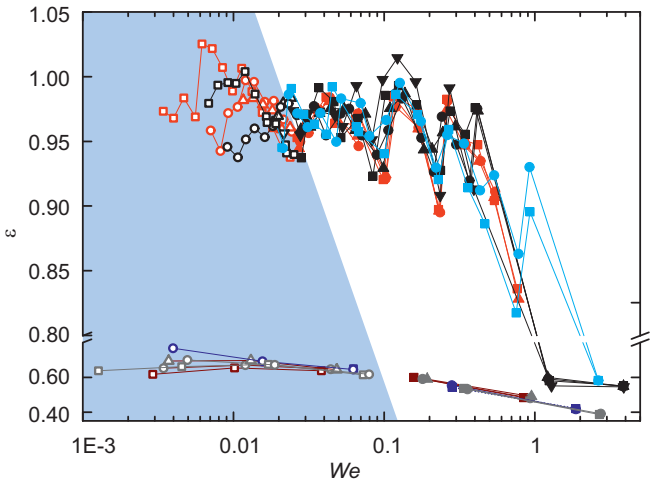

Figure S3| Restitution. Restitution coefficient versus We for bouncing series of water drops with $We_{init} = 0.76$ (red), 2.6 (cyan), and 3.9 (black); and glycerol drops with $We_{init} = 0.84$ (dark red), 1.9 (dark blue), and 2.7 (grey). Solid symbols denote bouncing, while open symbols (blue shaded region) denote hovering.

4. Dissipation in the viscous squeeze flow

We calculated the local dissipation rate within the air film using a standard lubrication calculation for the experimental film profiles (see Methods). The results are shown in Figure S4 as function of radial position and time. The dissipation rate is strongly peaked close to the kink along the edge of the drop where film thickness is minimum and the volumetric flow rate is high, while it is negligible in the dimple centre. Integrating these local rates over time and the drop-substrate interface yields the total air film dissipation. Because we miss part of the film profile just outside the kink – limited by the lateral resolution of the bottom view – our estimation of the total dissipation is conservative.

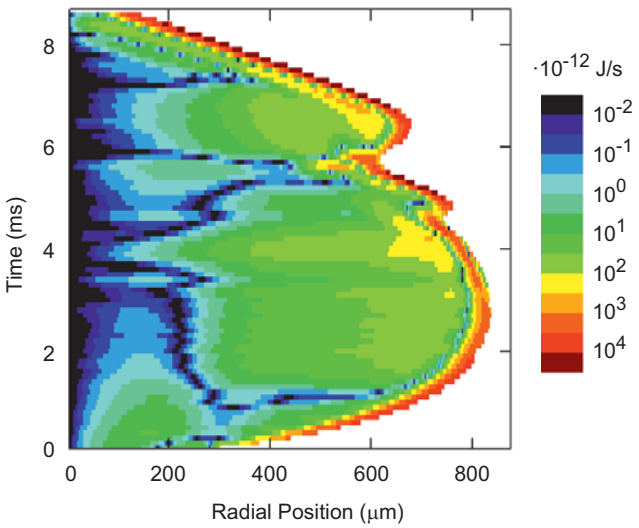

Figure S4| Dissipation rate map. Local dissipation rate in the air film as function of radial position and time for the air film profile shown in Figure 4a. The colour map ranges from blue (low) to red (high) dissipation, while steep interfacial slopes limit the determination to the central air film region (white outside).

5. Air film mediated bouncing on a nano-rough substrate

Finally, we performed experiments on glass wafers that are (super)hydrophobized by applying a nano-roughness in SU8 which is subsequently coated with a C_4F_8 layer, see also the Methods section. Movie S12 shows a bottom view recording of a bouncing water drop onto such a surface with 100 nm roughness amplitude (which is the maximum roughness value in these tests). Again, the interference patterns confirm that an air film with submicrometer thickness is present during the successive bouncing events. Finally the drop resides on the peaks of the structure in the Cassie-Baxter state with an advancing contact angle of 155°.

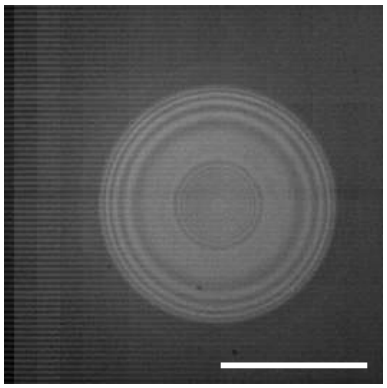

Movie S12| Air film mediated bouncing of a water drop on a nano-rough substrate. First bounce is at $W_{init} \approx$ 0.6 on a superhydrophobic substrate with a roughness amplitude of 100 nm (which also causes the poor contrast). The total timespan is 0.36 s (67× delayed). The scale bar is 1 mm.

References

1 Biance, A.-L., Chevy, F., Clanet, C., Lagubeau, G. & Quéré, D. On the elasticity of an inertial liquid shock. *J. Fluid Mech.* **554**, 47-66 (2006).